The Astrophysical Journal, 633:611–623, 2005 November 10

MODEL-INDEPENDENT MULTIVARIABLE GAMMA-RAY BURST LUMINOSITY INDICATOR AND ITS POSSIBLE COSMOLOGICAL IMPLICATIONS

Enwei Liang[1,2] and Bing Zhang[1]

Received 2005 April 18; accepted 2005 July 22

ABSTRACT

Without imposing any theoretical models and assumptions, we present a multivariable regression analysis to several observable quantities for a sample of 15 gamma-ray bursts (GRBs). The observables used in the analysis include the isotropic gamma-ray energy ($E_{\gamma,\rm iso}$), the peak energy of the νF_ν spectrum in the rest frame (E'_p), and the rest-frame break time of the optical afterglow light curves (t'_b). A strong dependence of $E_{\gamma,\rm iso}$ on E'_p and t'_b is derived, which reads $E_{\gamma,\rm iso}/10^{52}$ ergs $= (0.85 \pm 0.21)(E'_p/100\ \rm keV)^{1.94\pm0.17}(t'_b/1\ \rm day)^{-1.24\pm0.23}$ in a flat universe with $\Omega_M = 0.28$ and $H_0 = 71.3\ \rm km\ s^{-1}\ Mpc^{-1}$. We also extend the analysis to the isotropic afterglow energies in the X-ray and optical bands, respectively, and find that they are essentially not correlated with E'_p and t'_b. Regarding the $E_{\gamma,\rm iso}(E'_p,\ t'_b)$ relationship as a luminosity indicator, we explore the possible constraints on the cosmological parameters using the GRB sample. Since there is no low-redshift GRB sample to calibrate this relationship, we weight the probability of using the relationship in each cosmology to serve as a standard candle by χ^2 statistics and then use this cosmology-weighted standard candle to evaluate cosmological parameters. Our results indicate that $0.05 < \Omega_M < 0.50$ at the 1 σ level, with the most probable value of Ω_M being 0.28. The best value of Ω_Λ is 0.64, but it is less constrained. Only a loose limit of $\Omega_\Lambda < 1.2$ is obtained at the 1 σ level. In the case of a flat universe, the 1 σ constraints are $0.13 < \Omega_M < 0.49$ and $0.50 < \Omega_\Lambda < 0.85$, respectively. The deceleration factor (q) and its cosmological evolution (dq/dz) are also investigated with an evolutionary form of $q = q_0 + z\,dq/dz$. The best-fit values are $(q_0,\ dq/dz) = (-1.00,\ 1.12)$, with $-2.23 < q_0 < 0.26$ and $-0.07 < dq/dz < 3.48$ at the 1 σ level. The inferred transition redshift between the deceleration and acceleration phases is $0.78^{+0.32}_{-0.23}$ (1 σ). Through Monte Carlo simulations, we find that the GRB sample satisfying our relationship observationally tends to be a soft and bright one and that the constraints on the cosmological parameters can be much improved either by enlarging the sample size or by increasing the observational precision. Although the sample may not expand significantly in the *Swift* era, a significant increase of the sample is expected in the long-term future. Our simulations indicate that with a sample of 50 GRBs satisfying our multivariable standard candle, one can achieve a constraint to the cosmological parameters comparable to that derived from 157 Type Ia supernovae. Furthermore, the detections of a few high-redshift GRBs satisfying the correlation could greatly tighten the constraints. Identifying high-z GRBs and measuring their E'_p and t'_b are therefore essential for the GRB cosmology in the *Swift* era.

Subject headings: cosmological parameters — cosmology: observations — gamma rays: bursts

1. INTRODUCTION

Long gamma-ray bursts (GRBs) originate from cosmological distances (Metzger et al. 1997). Their births follow the star formation history of the universe (e.g., Totani 1997; Paczynski 1998; Bromm & Loeb 2002; Lin et al. 2004). GRBs therefore promise to serve as a new probe of cosmology and galaxy evolution (e.g., Djorgovski et al. 2003). It is well known that Type Ia supernovae (SNe Ia) are a perfect standard candle to measure the local universe up to a redshift of $\sim$2 (e.g., Riess et al. 2004). Gamma-ray photons (with energy from tens of keV to several MeV) from GRBs are almost immune to dust extinction. They should be detectable out to a very high redshift (Lamb & Reichart 2000; Ciardi & Loeb 2000; Gou et al. 2004). Hence, GRBs are potentially a more promising ruler than SNe Ia at higher redshifts.

This issue has attracted much attention in the GRB community. Frail et al. (2001) found that the geometrically corrected gamma-ray energy $E_{\rm jet}$ for long GRBs is narrowly clustered around 5×10^{50} ergs, suggesting that GRBs can potentially be a standard candle. A refined analysis by Bloom et al. (2003a) suggests that $E_{\rm jet}$ is clustered at 1.3×10^{51} ergs, but the dispersion of $E_{\rm jet}$ is too large for the purpose of constraining cosmological parameters. Schaefer (2003) considered two other luminosity indicators proposed earlier, i.e., the variability (Fenimore & Ramirez-Ruiz 2000; Reichart et al. 2001) and the spectral lag (Norris et al. 2000) for nine GRBs with known redshifts, and posed an upper limit of $\Omega_M < 0.35$ (1 σ) for a flat universe. Using 12 *BeppoSAX* bursts, Amati et al. (2002) found a relationship between the isotropic equivalent energy radiated during the prompt phase ($E_{\gamma,\rm iso}$) and the rest-frame peak energy in the GRB spectrum (E'_p), i.e., $E'_p \propto E^{1/2}_{\gamma,\rm iso}$. This relation was confirmed and extended to X-ray flashes by *High Energy Transient Explorer 2* (*HETE-2*) observations (Sakamoto et al. 2004; Lamb et al. 2005a). In addition, it also exists in the BATSE bursts (Lloyd et al. 2000) and even in different pulses within a single GRB (Liang et al. 2004). Possible theoretical explanations of this correlation have been proposed (Zhang & Mészáros 2002a; Dai & Lu 2002; Yamazaki et al. 2004; Eichler & Levinson 2004; Rees & Mészáros 2005). Because of a large dispersion, this relationship is not tight enough to serve as a standard candle for precision cosmology, either.

Ghirlanda et al. (2004a) found a tighter correlation between GRB jet energy and E'_p, which reads $E_{\rm jet} \propto (E'_p)^{3/2}$, where $E_{\rm jet} = E_{\gamma,\rm iso}(1 - \cos\theta_{\rm jet})$ and $\theta_{\rm jet}$ is the jet opening angle inferred from the "jet" break time imprinted in the light curves (usually in the

[1] Physics Department, University of Nevada, Las Vegas, NV 89154; lew@physics.unlv.edu, bzhang@physics.unlv.edu.
[2] Department of Physics, Guangxi University, Nanning 530004, China.

optical band, and in some cases in the X-ray and the radio bands) by assuming a uniform top-hat jet configuration. It is puzzling from the theoretical point of view how a global geometric quantity (jet angle) would conspire with $E_{\gamma,\rm iso}$ to affect E'_p. Nonetheless, the correlation has a very small scatter that is arguably fine enough to study cosmology. By assuming that the correlation is intrinsic, Dai et al. (2004) constrained the mass content of the universe to be $\Omega_M = 0.35 \pm 0.15$ in the case of a flat universe with a sample of 14 GRBs. They also constrained the dark matter equation-of-state parameter in the range of $w = -0.84^{+0.57}_{-0.83}$ at the 1 σ level. Ghirlanda et al. (2004b) evaluated the goodness of this relationship in different cosmologies by exploring the full cosmological parameter space and came up with similar conclusions. Friedman & Bloom (2005) suggested that this relationship is only marginal but not adequate enough for a precision cosmology study. The main criticisms are related to several assumptions involved in the current Ghirlanda relation, such as constant medium density (which could vary in different bursts; e.g., Panaitescu & Kumar 2002), constant radiative efficiency (which also varies from burst to burst; e.g., Lloyd-Ronning & Zhang 2004; Bloom et al. 2003a and references therein), and the assumption of the top-hat jet configuration (in principle jets are possibly structured; Rossi et al. 2002; Zhang & Mészáros 2002b). Nonetheless, the Ghirlanda relation has motivated much work on measuring cosmology with GRBs (e.g., Firmani et al. 2005; Qin et al. 2005; Xu et al. 2005; Xu 2005; Mortsell & Sollerman 2005).

In this work, we further address the GRB standard candle problem by a new statistical approach. Instead of sticking to the jet model and searching for the correlation between E'_p and $E_{\rm jet}$ (which requires a model- and parameter-dependent jet angle), we start with purely observable quantities to search for possible multivariable correlations by using a regression method. A similar technique was employed by Schaefer (2003). The motivations of our analysis are twofold. First, within the jet model, there is no confident interpretation to the Ghirlanda relation. It is relatively easy to imagine possible correlations between E'_p and $E_{\gamma,\rm iso}$ (e.g., Zhang & Mészáros 2002a; Rees & Mészáros 2005), since the latter is also a manifestation of the energy per solid angle along the line of sight, which could be possibly related to the emission spectrum. However, it is hard to imagine how the global geometry of the emitter would influence the local emission property.[3] Since there is no straightforward explanation for the Ghirlanda relation, one does not have to stick to this theoretical framework, but should rather try to look for some empirical correlations instead. This would allow more freedom for possible interpretations. Second, within various theoretical models (e.g., Table 1 of Zhang & Mészáros 2002a), the value of E'_p depends on multiple parameters. The problem is intrinsically multidimensional. It is pertinent to search for multivariable correlations rather than searching for correlations between two parameters only. The Ghirlanda relation is a relation that bridges the prompt emission and the afterglow phases. It is also worth checking whether or not there are similar relationships for other parameters. Below we perform a blind search for the possible multivariable correlations among several essential observable quantities, including the isotropic gamma-ray energy $E_{\gamma,\rm iso}$, the isotropic X-ray afterglow energy $E_{\rm XA,iso}$, the isotropic optical afterglow energy $E_{\rm OA,iso}$, the cosmological rest-frame peak energy E'_p, and the cosmological rest-frame temporal break in the *optical* afterglow light curve (t'_b). We describe our sample selection criteria and the data reduction method in § 2. Results of a multivariable regression analysis are presented in § 3. A strong dependence of $E_{\gamma,\rm iso}$ on E'_p and t'_b is derived from our multivariable regression analysis. Regarding the $E_{\gamma,\rm iso}(E'_p,\ t'_b)$ relationship as a luminosity indicator, in § 4 we explore the possible constraints on cosmological parameters using the GRB sample. In addition (§ 5), we perform Monte Carlo simulations to investigate the characteristics of the GRB sample satisfying the relationship observationally and examine how both the sample size and the observational precision affect the constraints on cosmological parameters. Conclusions and discussion are presented in § 6. Throughout the work the Hubble constant is adopted as $H_0 = 71.3$ km s^{-1} Mpc^{-1}.

[3] The simple Ghirlanda relation could be derived from the standard afterglow model and the Amati relation, but one has to assume that t'_b is constant for all GRBs, which is not true (see also Wu et al. 2004).

2. SAMPLE SELECTION AND DATA REDUCTION

Our sample includes 15 bursts with measurements of the redshift z, the spectral peak energy E_p, and the optical break time t_b. It has been suggested that the observed Amati relation and the Ghirlanda relation are likely due to some selection effects (Nakar & Piran 2005; Band & Preece 2005). The sample from which the relations are drawn may therefore be ill-defined if the parent sample is the whole GRB population. However, we believe that due to the great diversity of GRBs and their afterglow observations, one does not have to require all GRBs to form a global sample to serve as a standard candle. If one can identify a subclass of GRBs to act as a standard candle (such as SNe Ia in the supernova zoo), such a sample could give meaningful implications to cosmology. Our selected GRBs belong to such a category, which assemble a unique and homogeneous subclass. Since not all GRBs necessarily have an E_p or a t_b, the parent sample of our small sample is also only a subclass of the whole GRB population. Note that in order to preserve homogeneity, we do not include those bursts whose afterglow break times were observed in the radio band (GRB 970508, GRB 000418, GRB 020124) or in the X-ray band (GRB 970828) but were not seen in the optical band. Since we are not sticking to the jet model, we do not automatically accept that there should be a temporal break as well in the optical band. We also exclude those bursts whose E_p or t_b are not directly measured (but with upper or lower limits inferred from theoretical modeling). This gives a sample of 15 bursts up to 2005 February. They are tabulated in Table 1 with the following headings: (1) GRB name; (2) redshift; spectral fitting parameters including (3) spectral peak energy E_p (with error σ_{E_p}), (4) low-energy spectral index α, and (5) high-energy spectral index β; (6) γ-ray fluence (S_γ) normalized to a standard band pass (1–10^4 keV in the cosmological rest frame) according to spectral fitting parameters (with error $[\sigma_{S_\gamma}]$); (7) the corresponding observation energy band; and (8) references for these observational data. Our GRB sample essentially resemble those used in Ghirlanda et al. (2004a), Dai et al. (2004), and Xu et al. (2005). These bursts are included in the Table 1 of Friedman & Bloom (2005), but that table also includes those bursts with only limits for E_p, t_j, and z, as well as those bursts whose t_b was observed in the nonoptical bands (or inferred from theoretical model fittings). We believe that our sample is more homogeneous than the sample listed in Friedman & Bloom (2005).

The X-ray and optical afterglow data of these GRBs are listed in Table 2 with the following headings: (1) GRB name; (2) X-ray afterglow temporal decay index, $\alpha_{\rm X}$; (3) epoch of X-ray afterglow observation (in units of hours); (4) 2–10 keV X-ray flux ($F_{\rm X}$, in units of 10^{-13} ergs cm $^{-2}$ s $^{-1}$) at the corresponding

TABLE 1

PROMPT EMISSION PARAMETERS OF THE GRB SAMPLE ADOPTED IN THIS PAPER

GRB (1)	z (2)	$E_p(\sigma_{E_p})$ (keV) (3)	α (4)	β (5)	$S_\gamma(\sigma_S)$ (ergs cm^{-2}) (6)	Band (keV) (7)	References (8)
980703	0.966	254(50.8)	−1.31	−2.40	22.6(2.3)	20–2000	1; 2; 2; 2
990123	1.6	780.8(61.9)	−0.89	−2.45	300(40)	40–700	3; 4; 4; 4
990510	1.62	161.5(16.1)	−1.23	−2.70	19(2)	40–700	5; 4; 4; 4
990712	0.43	65(11)	−1.88	−2.48	6.5(0.3)	40–700	5; 4; 4; 4
991216	1.02	317.3(63.4)	−1.23	−2.18	194(19)	20–2000	6; 2; 2; 2
011211	2.14	59.2(7.6)	−0.84	−2.30	5.0(0.5)	40–700	7; 8; 8; 7
020124	3.2	86.9(15.0)	−0.79	−2.30	8.1(0.8)	2–400	9; 10; 10; 10
020405	0.69	192.5(53.8)	0.00	−1.87	74.0(0.7)	15–2000	11; 11; 11; 11
020813	1.25	142(13)	−0.94	−1.57	97.9(10)	2–400	12; 10; 10; 10
021004	2.332	79.8(30)	−1.01	−2.30	2.6(0.6)	2–400	13; 10; 10; 10
021211	1.006	46.8(5.5)	−0.86	−2.18	3.5(0.1)	2–400	14; 10; 10; 10
030226	1.986	97(20)	−0.89	−2.30	5.61(0.65)	2–400	15; 10; 10; 10
030328	1.52	126.3(13.5)	−1.14	−2.09	37.0(1.4)	2–400	16; 10; 10; 10
030329	0.1685	67.9(2.2)	−1.26	−2.28	163(10)	2–400	17; 10; 10; 10
030429	2.6564	35(9)	−1.12	−2.30	0.85(0.14)	2–400	18; 10; 10; 10

REFERENCES.—References are in order for z, $E_p^{\rm obs}$, (α, β), S_γ: (1) Djorgovski et al. 1998; (2) Jimenez et al. 2001; (3) Kulkarni et al. 1999; (4) Amati et al. 2002; (5) Vreeswijk et al. 2001; (6) Djorgovski et al. 1999; (7) Holland et al. 2002; (8) Amati 2003; (9) Hjorth et al. 2003; (10) Sakamoto et al. 2005; (11) Price et al. 2003; (12) Barth et al. 2003; (13) Möller et al. 2002; (14) Vreeswijk et al. 2003; (15) Greiner et al. 2003; (16) Martini et al. 2003; (17) Bloom et al. 2003b; (18) Weidinger et al. 2003.

epoch; (5) 2–10 keV X-ray afterglow flux normalized to 10 hours after the burst trigger (including the error); (6) temporal break (including the error) of the optical afterglow light curves (t_b); (7) optical temporal decay index before the break (α_1); (8) optical temporal decay index after the break (α_2); (9) references; (10) R-band optical afterglow magnitudes at 11 hours. We find that the mean values of $\alpha_{\rm X}$, α_1, and α_2 in our sample are 1.41, 1.0, and 2.0, respectively. For those bursts whose $\alpha_{\rm X}$, α_1, and α_2 values are not available, we take these means in our calculation.

With the data collected in Tables 1 and 2, we calculate the total isotropic emission energies in the gamma-ray prompt phase ($E_{\gamma,\rm iso}$), in the X-ray afterglow ($E_{\rm XA,iso}$), and in the optical afterglow (R band) ($E_{\rm OA,iso}$), i.e.,

$$E_{\gamma,\rm iso} = \frac{4\pi D_L^2(z) S_\gamma k}{1+z}, \quad (1)$$

$$E_{\rm XA,iso} = \frac{4\pi D_L^2(z) \int_{t_1}^{t_2} F_x(t_1) t^{\alpha_{\rm X}}\, dt}{1+z}, \quad (2)$$

TABLE 2

X-RAY AND OPTICAL AFTERGLOW DATA OF THE GRB SAMPLE ADOPTED IN THIS PAPER

GRB (1)	$\alpha_{\rm X}$[a] (2)	Epoch[a] (hr) (3)	$F_{\rm X}$[a] (4)	$F_{\rm X,10\ hr}$ ($\sigma_{F_{\rm X,10\ hr}}$)[a] (5)	$t_b(\sigma_{t_b})$[b] (days) (6)	α_1[b] (7)	α_2[b] (8)	Reference[b] (9)	$R_{11\ \rm hr}$[c] (10)
980703	1.24	34	4	18.24(4.97)	3.4(0.5)	...	...	1	20.1
990123	1.08	6	110	66.09(6.33)	2.04(0.46)	1.17	1.57	2	19.4
990510	1.41	8.7	47.8	41.07(3.68)	1.6(0.2)	0.46	1.85	3	18.1
990712	...	...	...	...	1.6(0.2)	0.83	3.06	4	19.5
991216	1.61	4	1240	287.21(14.73)	1.2(0.4)	1	1.8	5	16.9
011211	1.5	11	1.9	2.23(0.39)	1.56(0.02)	0.95	2.11	6	20.1
020124	...	...	...	...	3(0.4)	...	...	7	21.6
020405	1.15	41	13.6	68.98(20.21)	1.67(0.52)	1.4	1.95	8	18.3
020813	1.42	39	22	113.98(17.01)	0.43(0.06)	0.76	1.46	9	19.1
021004	1.56	20.81	4.3	13.5(2.47)	4.74(0.14)	0.85	1.43	10	18.4
021211	...	...	...	...	1.4(0.5)	...	...	11	21.3
030226	...	37.1	0.32	12.3	1.04(0.12)	0.77	1.99	12	19.5
030328	...	15.33	3	...	0.8(0.1)	1.0	1.6	13	20.2
030329	1.74	4.85	1400	467(23)	0.5(0.1)	1.18	1.81	14	14.7
030429	...	...	...	...	1.77(1)	0.88	2.87	15	20.2

[a] Temporal decay index and X-ray afterglow flux in the 2–10 keV band at a given observed epoch. $F_{\rm X,10\ hr}$ is the extrapolated/interpolated X-ray afterglow flux at 10 hours after the GRB trigger. The fluxes are in units of 10^{-13} ergs cm^{-2} s^{-1}. They are taken from Berger et al. (2003) except for those with marks: 030226 (Pedersen et al. 2003); 030328 (Butler et al. 2003); 030329 (Marshall & Swank 2003; Marshall et al. 2003; Tiengo et al. 2003a, 2003b).

[b] Temporal break (error) and temporal indices before and after the break, and their references: (1) Frail et al. 2003; (2) Kulkarni et al. 1999; (3) Stanek et al. 1999; (4) Björnsson et al. 2001; (5) Halpern et al. 2000; (6) Jakobsson et al. 2003; (7) Berger et al. 2002; (8) Price et al. 2003; (9) Barth et al. 2003; (10) Holland et al. 2003; (11) Holland et al. 2004; (12) Klose et al. 2004; (13) Andersen et al. 2003; (14) Berger et al. 2003; (15) Jakobsson et al. 2004a.

[c] R-band magnitude adjusted to 11 hr after the burst trigger (from Jakobsson et al. 2004b).

TABLE 3
Derived Isotropic Energies, Rest-Frame Peak Energies, and Rest-Frame Temporal Breaks for the GRB Sample Adopted in this Paper (for $\Omega_M = 0.28$ and $\Omega_\Lambda = 0.72$)

GRB (1)	$\log E_{\gamma,\rm iso}(\sigma_{E_\gamma})$ (ergs) (2)	$\log E_{\rm XA,iso}$ (ergs) (3)	$\log E_{\rm OA,iso}$ (ergs) (4)	$\log E'_p(\sigma_{E_p})$ (keV) (5)	$\log t'_b(\sigma_{t_b})$ (day) (5)
980703	52.85(0.04)	47.69	...	2.70(0.09)	0.238(0.064)
990123	54.64(0.06)	48.80	46.09	3.31(0.03)	−0.105(0.098)
990510	53.29(0.05)	48.58	46.60	2.63(0.04)	−0.222(0.008)
990712	51.88(0.02)	...	44.08	1.97(0.07)	0.049(0.054)
991216	53.85(0.04)	49.00	45.70	2.81(0.09)	−0.226(0.145)
011211	53.01(0.04)	47.72	45.84	2.27(0.06)	−0.304(0.006)
020124	53.37(0.05)	...	...	2.70(0.08)	−0.146(0.058)
020405	53.17(0.01)	47.92	45.91	2.51(0.12)	−0.005(0.135)
020813	54.13(0.06)	48.90	45.42	2.68(0.09)	−0.719(0.061)
021004	52.66(0.10)	48.54	46.82	2.42(0.16)	0.153(0.013)
021211	52.05(0.03)	...	...	1.97(0.05)	−0.156(0.155)
030226	52.90(0.05)	47.52	46.14	2.46(0.09)	−0.458(0.050)
030328	53.60(0.02)	47.66	45.51	2.50(0.05)	−0.498(0.054)
030329	52.19(0.04)	48.27	45.40	1.90(0.01)	−0.369(0.087)
030429	52.24(0.07)	...	46.30	2.11(0.11)	−0.315(0.245)

and

$$E_{\rm OA,iso} = \frac{4\pi D_L^2(z)\left[\int_{t_1}^{t_b} F_R(t_1)t^{\alpha_1}\,dt + \int_{t_b}^{t_2} F_R(t_b)t^{\alpha_2}\,dt\right]}{1+z}. \quad (3)$$

Here $D_L(z)$ is the luminosity distance at the redshift z, k is a k-correction factor to correct the observed gamma-ray fluence at an observed bandpass to a given bandpass in the cosmological rest frame (1–10^4 keV in this analysis), t_1 and t_2 are, respectively, the starting and the ending times of the afterglow phase, F_X is the flux of the X-ray afterglow in the 2–10 keV band, and F_R is the flux of the optical afterglow in the R band ($F_R = \nu_R f_\nu$). Since the very early afterglows might be significantly different from the later afterglows, which were not directly detected for the GRBs in our sample, we thus take $t_1 = 1$ hr. We also choose $t_2 = 30$ days. The derived $E_{\gamma,\rm iso}$, $E_{\rm XA,iso}$, and $E_{\rm OA,iso}$ are tabulated in Table 3.

3. MULTIVARIABLE REGRESSION ANALYSIS

As mentioned in § 1, previous authors interpret the relationship among $E_{\gamma,\rm iso}$, E'_p, and t'_b based on the GRB jet model (e.g., Rhoads 1999; Sari et al. 1999). In this scenario, the relationship among the three quantities becomes the $E_{\rm jet} \propto (E'_p)^{3/2}$ relationship. When this relation is expanded, one gets $E_{\gamma,\rm iso}t'_b \propto (E'_p)^2$. The indices for $E_{\gamma,\rm iso}$ and t'_b are not independent and are bound by the jet model. However, since the current jet model is difficult to accommodate the $E_{\rm jet}$-E_p relationship, we no longer need to assume an underlying correlation between $E_{\gamma,\rm iso}$ and t'_b. We therefore leave all the indices as free parameters and perform a multivariable regression analysis to search a possible empirical relationship among $E_{\gamma,\rm iso}$, E'_p, and t'_b. We also extend our analysis to search the dependence of $E_{X,\rm iso}$ and $E_{R,\rm iso}$ on E'_p and t'_b, respectively. The regression model we use reads

$$\hat{E}_{\rm iso} = 10^{\kappa_0} E_p'^{\kappa_1} t_b'^{\kappa_2}, \quad (4)$$

where $E'_p = E_p(1+z)$ and $t'_b = t_b/(1+z)$. We measure the significance level of the dependence of each variable on the model by the probability of a t-test (p_t). The significance of the global regression is measured by an F-test (the F-test statistics and the corresponding significance level p_F) and a Spearman linear correlation between $\log \hat{E}_{\rm iso}$ and $\log E_{\rm iso}$ (the correlation coefficient r and the significance level p_S). We find that $E_{\gamma,\rm iso}$ strongly depends on both E'_p and t'_b with a very small uncertainty (Table 4, Fig. 1). The actual dependence format depends on the cosmology adopted. For a flat universe with $\Omega_M = 0.28$, this relation reads

$$\hat{E}_{\gamma,\rm iso,52} = (0.85 \pm 0.21)\left(\frac{E'_p}{100\ \rm keV}\right)^{1.94\pm0.17}\left(\frac{t'_b}{1\ \rm day}\right)^{-1.24\pm0.23}, \quad (5)$$

TABLE 4
Results of Multiple Variable Regression Analysis (for $\Omega_M = 0.28$ and $\Omega_\Lambda = 0.72$)

Parameter	$\hat{E}_{\gamma,\rm iso}(E'_p, t'_b)$	$\hat{E}_{\rm X,iso}(E'_p, t'_b)$	$\hat{E}_{R,\rm iso}(E'_p, t'_b)$
$\kappa_0(p_t)$	$48.0 \pm 0.4(<10^{-4})$	$46.27 \pm 1.35(<10^{-4})$	$44.22 \pm 1.42(<10^{-4})$
$\kappa_1(p_t)$	$1.94 \pm 0.17(<10^{-4})$	$0.74 \pm 0.51(0.18)$	$0.64 \pm 0.57(0.26)$
$\kappa_2(p_t)$	$-1.24 \pm 0.23(2\times10^{-4})$	$-0.30 \pm 0.62(0.64)$	$0.29 \pm 0.88(0.75)$
Global F-test statistics	115.4	1.08	0.77
Probability p_F	$<10^{-4}$	0.39	0.49
Global correlation r	0.96 ± 0.21	0.46 ± 0.24	0.38 ± 0.28
Probability P_S	$<10^{-4}$	0.15	0.22

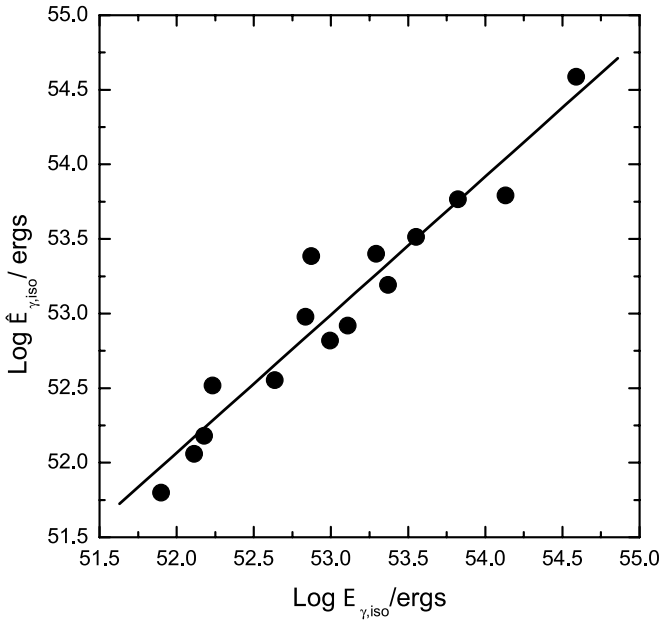

FIG. 1.—Plot of log $\hat{E}_{\gamma,\rm iso}$ calculated by the empirical relationship from our multivariable regression analysis as compared with log $E_{\gamma,\rm iso}$ derived from the observed fluence with the cosmological parameters of $\Omega_M = 0.28$ and $\Omega_\Lambda = 0.72$. The solid line is the regression line for the two quantities.

where $\hat{E}_{\gamma,\rm iso,52} = \hat{E}_{\gamma,\rm iso}/10^{52}$ ergs. However, when we test the possible correlations among $E_{\rm X,iso}$ (or $E_{o,\rm iso}$), E'_p, and t'_b, no significant correlation is found (Table 4, Figs. 2 and 3).

4. LUMINOSITY INDICATOR AND COSMOLOGICAL IMPLICATIONS

The dispersion of the $\hat{E}_{\gamma,\rm iso}(E'_p,\ t'_b)$ relationship is so small that it could potentially serve as a luminosity indicator for the cosmological study. This relationship is *purely empirical*, exclusively using directly measured quantities, and without imposing any theoretical models and assumptions. It therefore suffers fewer uncertainties/criticisms than does the Ghirlanda relation (e.g., Friedman & Bloom 2005). Below we discuss the cosmological implications for this new empirical luminosity indicator.

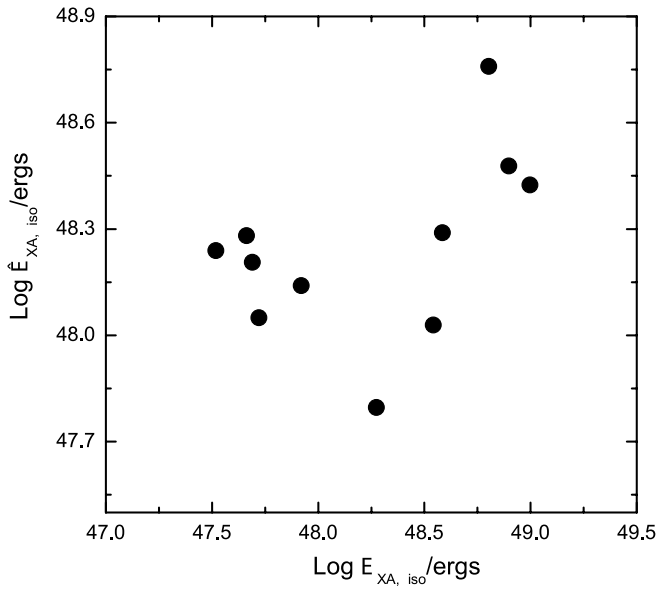

FIG. 2.—Plot of log $\hat{E}_{\rm XA,iso}$ calculated by the empirical relationship from our multivariable regression analysis as compared with log $E_{\rm XA,iso}$ derived with the cosmological parameters of $\Omega_M = 0.28$ and $\Omega_\Lambda = 0.72$.

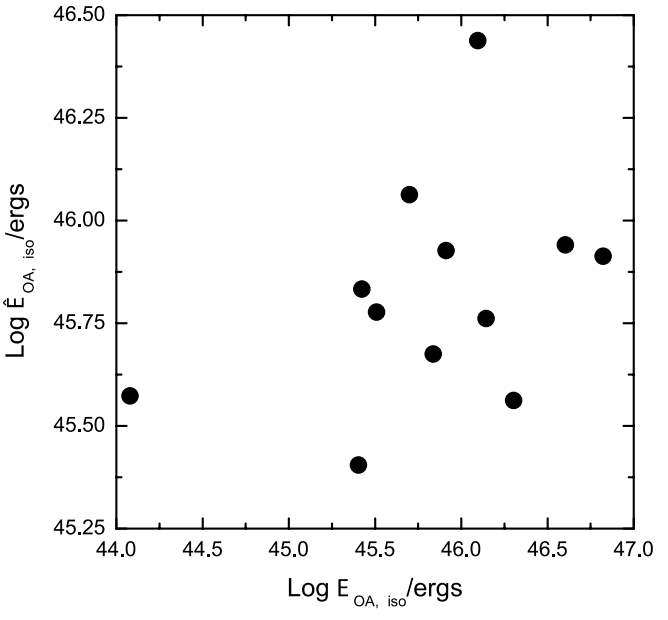

FIG. 3.—Plot of log $\hat{E}_{\rm OA,iso}$ calculated by the empirical relationship from our multivariable regression analysis as compared with log $E_{\rm OA,iso}$ derived with the cosmological parameters of $\Omega_M = 0.28$ and $\Omega_\Lambda = 0.72$.

The distance modulus of a GRB, which is defined as $\mu \equiv 5 \log (D_L/10\ \rm pc)$, could be measured by this luminosity indicator as

$$\hat{\mu} = 2.5\left[\kappa_0 + \kappa_1 \log E'_p + \kappa_2 \log t'_b - \log\left(4\pi S_\gamma k\right) + \log\left(1+z\right)\right] - 97.45. \quad (6)$$

Since the luminosity indicator is cosmology-dependent, $\hat{\mu}$ is also cosmology-dependent. We therefore cannot directly use this relationship for our purpose. Ideally, it should be calibrated by local GRBs (e.g., $z < 0.1$), as is the case of Type Ia supernova cosmology. However, the GRB low redshift sample is small. More importantly, the local GRBs appear to have different characteristics than the cosmological ones (e.g., long lag, less luminous), so that they may not belong to the subclass of GRBs we are discussing. We are left out without a *real* (cosmology-independent) luminosity indicator at this time.

We adopt the following method to circumvent the difficulty. We first recalibrate this relationship in each cosmological model, and then calculate the goodness of the relationship in that cosmology by χ^2 statistics. We then construct a relation that is weighted by the goodness of each cosmology-dependent relationship, and use this cosmology-weighted relationship to measure the universe. The procedure to calculate the probability function of a cosmological parameter set (denoted as Ω, which includes both Ω_M and Ω_Λ) is the following.

1. Calibrate and weight the luminosity indicator in each cosmology. Given a particular set of cosmological parameters ($\bar{\Omega}$), we perform a multivariable regression analysis and get a best-fit correlation $\hat{E}_{\gamma,\rm iso}(\bar{\Omega};\ E'_p,\ t'_b)$. We evaluate the probability $[w(\bar{\Omega})]$ of using this relation as a cosmology-independent luminosity indicator via χ^2 statistics, i.e.,

$$\chi^2_w(\bar{\Omega}) = \sum_i^N \frac{\left[\log \hat{E}^i_{\gamma,\rm iso}(\bar{\Omega}) - \log E^i_{\gamma,\rm iso}(\bar{\Omega})\right]^2}{\sigma^2_{\log \hat{E}^i_{\gamma,\rm iso}}(\bar{\Omega})}. \quad (7)$$

The smaller the χ_r^2, the better the fit and hence, the higher the probability for this cosmology-dependent relationship to serve as a cosmology-independent luminosity indicator. We assume that the distribution of the $\chi_w^2(\bar{\Omega})$ is normal, so the probability can be calculated as

$$w(\bar{\Omega}) \propto e^{-\chi_w^2(\bar{\Omega})/2}. \quad (8)$$

2. Regard the $\hat{E}_{\gamma,\mathrm{iso}}(\bar{\Omega};\ E'_p,\ t'_b)$ relationship derived in each cosmology as a cosmology-independent luminosity indicator without considering its systematic error and calculate the corresponding distance modulus $\hat{\mu}(\bar{\Omega})$ (eq. [6]) and its error $\sigma_{\hat{\mu}}$, which is

$$\sigma_{\hat{\mu}_i} = \frac{2.5}{\ln 10}\left[\left(\kappa_1 \frac{\sigma_{E'_{p,i}}}{E'_{p,i}}\right)^2 + \left(\kappa_2 \frac{\sigma_{t'_{b,i}}}{t'_{b,i}}\right)^2 + \left(\frac{\sigma_{S_{\gamma,i}}}{S_{\gamma,i}}\right)^2 + \left(\frac{\sigma_{k_i}}{k_i}\right)^2 + \left(\frac{\sigma_{z_i}}{1+z_i}\right)^2\right]^{1/2}. \quad (9)$$

3. Calculate the theoretical distance modulus $\mu(\Omega)$ in an arbitrary set of cosmological parameters (denoted by Ω) and calculate the χ^2 of $\mu(\Omega)$ against $\hat{\mu}(\Omega)$, i.e.,

$$\chi^2(\bar{\Omega}|\Omega) = \sum_i^N \frac{\left[\hat{\mu}_i(\bar{\Omega}) - \mu_i(\Omega)\right]^2}{\sigma^2_{\hat{\mu}_i}(\bar{\Omega})}. \quad (10)$$

4. Assuming that the distribution of $\chi^2(\bar{\Omega}|\Omega)$ is also normal, calculate the probability that the cosmology parameter set Ω is the right one according to the luminosity indicator derived from the cosmological parameter set $\bar{\Omega}$, i.e.,

$$p(\bar{\Omega}|\Omega) \propto e^{-\chi^2(\bar{\Omega}|\Omega)/2}. \quad (11)$$

With equation (8), we can define a cosmology-weighted likelihood by $w(\bar{\Omega})p(\bar{\Omega}|\Omega)$.

5. Integrate $\bar{\Omega}$ over the full cosmology parameter space to get the final normalized probability that the cosmology Ω is the right one, i.e.,

$$p(\Omega) = \frac{\int_{\bar{\Omega}} w(\bar{\Omega}) p(\bar{\Omega}|\Omega)\, d\bar{\Omega}}{\int_{\bar{\Omega}} w(\bar{\Omega})\, d\bar{\Omega}}. \quad (12)$$

In our calculation, the integration in equation (12) is computed through summing over a wide range of the cosmology parameter space to make the sum converge, i.e.,

$$p(\Omega) = \frac{\sum_{\bar{\Omega}_i} w(\bar{\Omega}_i) p(\bar{\Omega}_i|\Omega)}{\sum_{\bar{\Omega}_i} w(\bar{\Omega}_i)}. \quad (13)$$

The essential ingredient of our method is that we do not include the systematical error of the $\hat{E}_{\gamma,\mathrm{iso}}(\bar{\Omega};\ E'_p,\ t'_b)$ relationship into $\sigma_{\hat{\mu}_{s,i}}$. Instead, we evaluate the probability that a particular relationship can be served as a cosmology-independent luminosity indicator using its systematical error, and integrate over the full cosmology parameter space to get the final probability of a cosmology with the parameter set Ω. In Figure 4 we plot $\hat{\mu}$ against μ with $\sigma_{\hat{\mu}_s}$ in the case of $\Omega = 0.28$ and $\Omega_\Lambda = 0.72$ cosmology. Similar investigation could be done for other cosmologies. Below, we apply the approach discussed above to investigate the possible implications on cosmography and cosmological dynamics with our GRB sample.

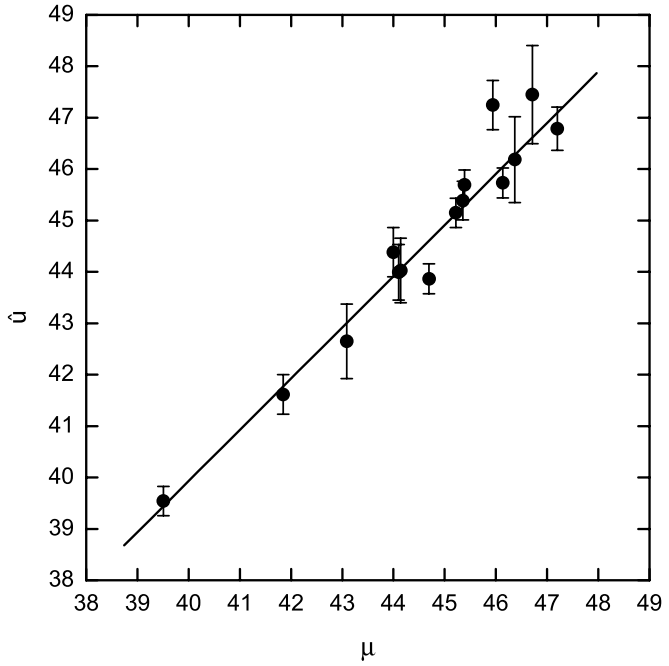

FIG. 4.—Distance modulus derived from the data, $\hat{\mu}$, and its observational error, $\sigma_{\hat{\mu}}$, plotted against the distance modulus derived from theory, μ. The cosmological parameters adopted are $\Omega_M = 0.28$ and $\Omega_\Lambda = 0.72$.

4.1. *Implications for Ω_M and Ω_Λ*

In a Friedmann-Robertson-Walker (FRW) cosmology with mass density Ω_M and vacuum energy density Ω_Λ, the luminosity distance is given by

$$D_L = c(1+z)H_0^{-1}|\Omega_k|^{-1/2}\,\mathrm{sinn}\left\{|\Omega_k|^{1/2} \times \int_0^z dz\left[(1+z)^2(1+\Omega_M z) - z(2+z)\Omega_\Lambda\right]^{-1/2}\right\}, \quad (14)$$

where c is the speed of light, H_0 is the present Hubble constant, $\Omega_k = 1 - \Omega_M - \Omega_\Lambda$ denotes the curvature of the universe, and "sinn" is sinh for $\Omega_k > 0$ and sin for $\Omega_k < 0$. For a flat universe ($\Omega_k = 0$), equation (14) turns out to be $c(1+z)H_0^{-1}$ times the integral. We calculate $p(\Omega)$ with our GRB sample, where $\Omega = (\Omega_M,\ \Omega_\Lambda)$. Since both $[\sigma_z/(1+z)]^2$ and $(\sigma_k/k)^2$ are significantly smaller than the other terms in equation (9), they are ignored in our calculations. Shown in Figure 5 are the most probable value of $(\Omega_M,\ \Omega_\Lambda)$ and the 1 σ to 3 σ contours of the likelihood in the $(\Omega_M,\ \Omega_\Lambda)$-plane. The most probable value of $(\Omega_M,\ \Omega_\Lambda)$ is (0.28, 0.64). The contours show that $0.05 < \Omega_M < 0.50$ at 1 σ, but Ω_Λ is poorly constrained; i.e., $\Omega_\Lambda < 1.2$ at 1 σ. For a flat universe, as denoted as the dashed line in Figure 5, the constraints are tighter, i.e., $0.13 < \Omega_M < 0.49$ and $0.50 < \Omega_\Lambda < 0.85$ at 1 σ.

4.2. *Implications for the Cosmology Dynamics*

Riess et al. (2004) found the evidence from SNe Ia data that the universe was switched from a past decelerating phase to the currently accelerating phase at an epoch of $z_t = 0.46 \pm 0.13$, assuming that the deceleration factor q evolves with redshift as

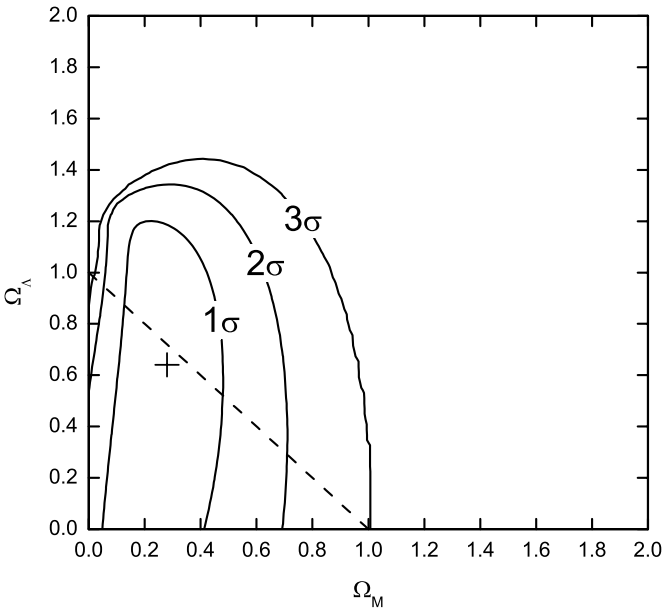

FIG. 5.—Contours of likelihood interval distributions in the (Ω_M, Ω_Λ)-plane inferred from the current GRB sample using the method developed in § 4. The cross marks the most probable value of (Ω_M, Ω_Λ), which is (0.28, 0.64). The contours give $0.05 < \Omega_M < 0.50$ (1 σ). Considering a flat universe (*dashed line*), the contours yield $0.13 < \Omega_M < 0.49$ and $0.50 < \Omega_\Lambda < 0.85$ (1 σ).

$q(z) = q_0 + z\,dq/dz$. Following Riess et al. (2004), we also take $q(z) = q_0 + z\,dq/dz$ to analyze the implications for q_0 and dq/dz from the current GRB sample. The luminosity distance in a (q_0, dq/dz) model can be written as

$$D_L = \frac{c(1+z)}{H_0}\int_0^z e^{-\int_0^u [1+q(u)]d\,\ln(1+u)}\,du. \qquad (15)$$

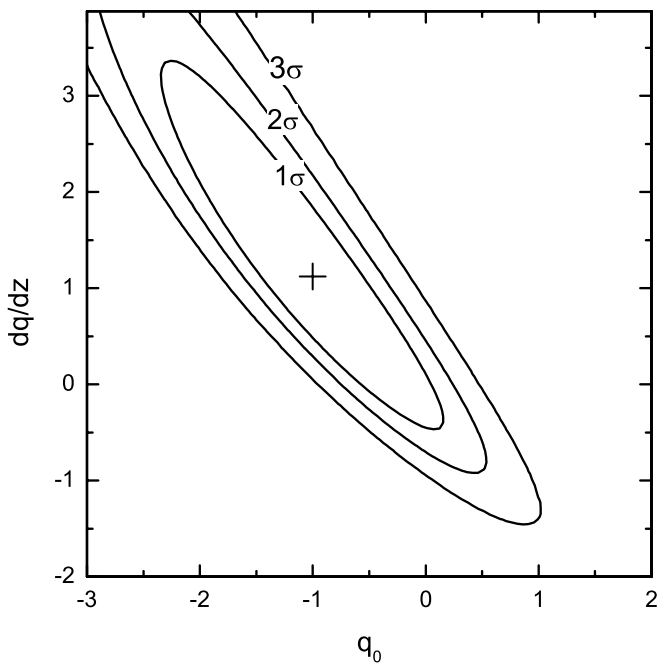

FIG. 6.—Contours of likelihood interval distributions in the (q_0, dq/dz)-plane inferred from the current GRB sample using the method developed in § 4. The most probable values of (q_0, dq/dz) are (−1.00, 1.12) (*plus sign*). At the 1 σ level their values are constrained in the ranges of $-2.23 < q_0 < 0.26$ and $-0.07 < dq/dz < 3.48$, respectively.

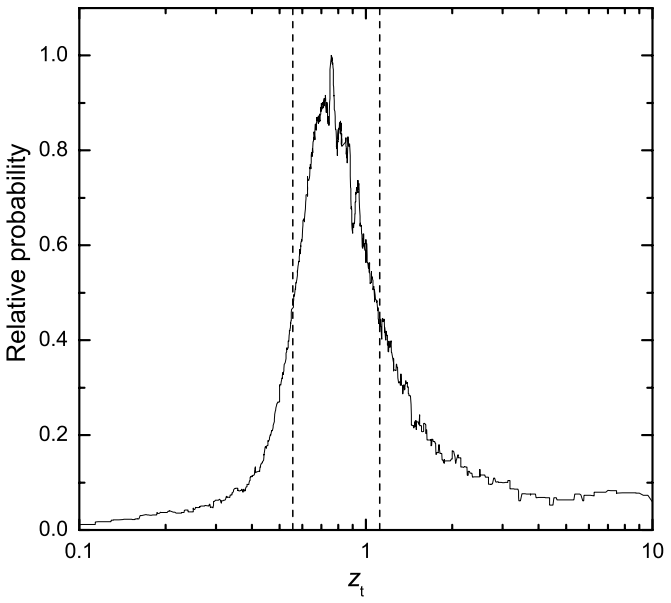

FIG. 7.—Smoothed likelihood function of the transition redshift from a decelerating universe to an accelerating universe inferred from the current GRB sample. The dashed lines mark the 1 σ region, and the best value of $\hat{z}_t$ is $0.78^{+0.32}_{-0.23}$.

We then calculate the values of $P(\Omega)$ [where $\Omega = (q_0,\ dq/dz)$] using the cosmology-weighted standard candle method discussed above. Shown in Figure 6 are the most probable values of (q_0, dq/dz) and their likelihood interval contours from 1 to 3 σ. The most probable values of (q_0, dq/dz) are (−1.0, 1.12), and at the 1 σ level their values are constrained in the ranges of $-2.23 < q_0 < 0.26$ and $-0.07 < dq/dz < 3.48$. Although the current sample still does not place a tight constraint on both q_0 and dq/dz, it shows that q_0 tends to be less than 0 and dq/dz tends to be greater than 0, suggesting that the universe is accelerating now. At a given epoch z_t in the past, $q(z_t) = 0$ should be satisfied, which denotes the transition between the past decelerating phase and the currently accelerating phase. The likelihood function of z_t derived from the current GRB sample is shown in Figure 7. We calculate the best value of z_t by

$$\hat{z}_t = \frac{\sum p(z_t) z_t}{\sum p(z_t)}, \qquad (16)$$

and get $\hat{z}_t = 0.78^{+0.32}_{-0.23}$ at 1 σ.

5. SIMULATIONS

We have shown that using the analysis method proposed in this paper, one can place some constraints on the cosmology parameters with our GRB sample. These constraints are, however, weaker than those obtained with the SNe Ia data, and they have uncertainties because of the small GRB sample effect. To increase the significance of the constraints, one needs a larger sample and smaller error bars for the measurements. In order to access the characteristics of the GRB sample satisfying our relationship observationally and how the sample size and the measurement precision affect the standard analysis, we perform some Monte Carlo simulations. We simulate a sample of 10^3 GRBs. Each burst is characterized by a set of parameters denoted as (z, E_p, S_γ, t_b). A fluence threshold of $S_{\mathrm{th},\gamma} = 10^{-7}$ ergs s^{-1} is adopted. Since the observed t_b is in the range of 0.4–6 days, we also require that t_b be in the same range to account for the

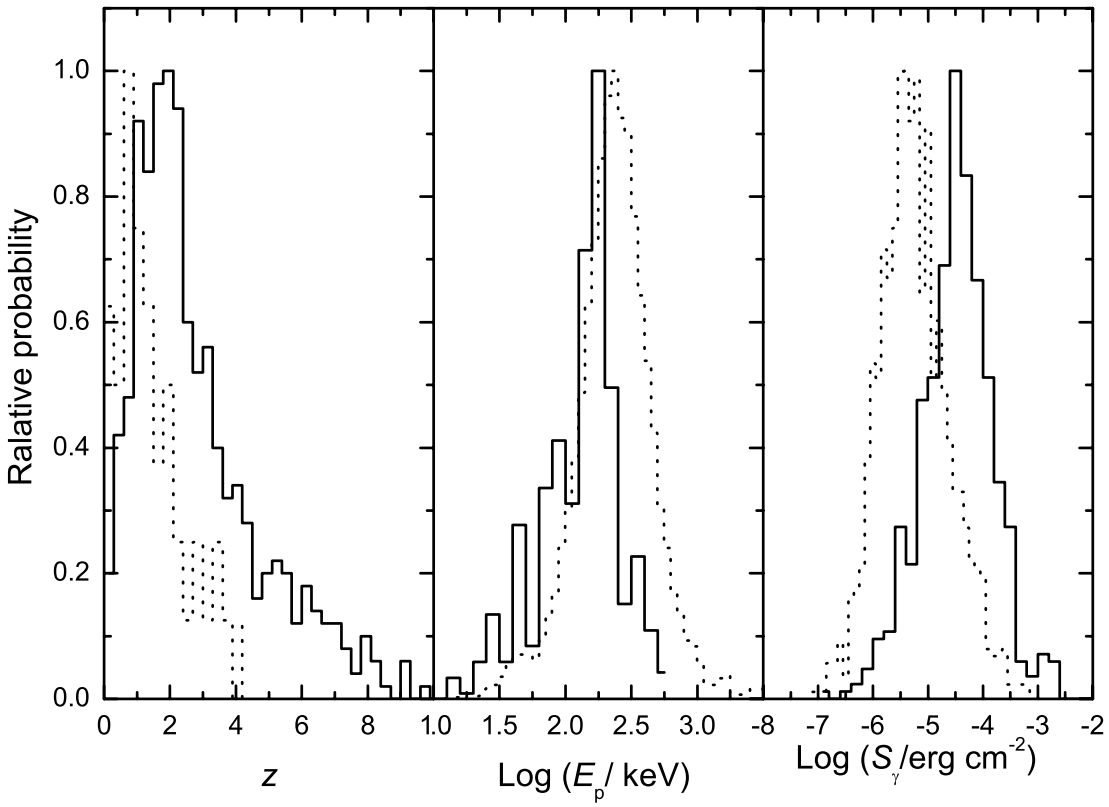

FIG. 8.—Distributions of z, E_p, and S_γ for the simulated GRB sample satisfying our model-independent standard candle relationship. For comparison, the superposed dotted lines are the distributions derived from the observational data.

selection effect to measure an optical light curve break. Our simulation procedures are described as follows.

1. Model the cumulative probability distributions of E_p, $E_{\rm iso}$, and z by the observational data. We first obtain the differential distribution of these measurements. The E_p distribution is derived from the GRB spectral catalog presented by Preece et al. (2000), which is well modeled by $dp/d\log E_p \propto \exp[-2(\log E_{p,2} - 0.38)^2/0.45^2]$, where $E_{p,2} = E_p/100$ (Liang et al. 2004). The $E_{\rm iso}$ distribution is obtained from the current sample of GRBs with known redshifts. Since the $E_{\rm iso}$ distribution suffers observational bias at the low $E_{\rm iso}$ end, we consider only those bursts with $E_{\rm iso} > 10^{51.5}$ ergs and get $dp/d\log E_{\rm iso} \propto -0.3\log E_{\rm iso}$.[4] The redshift distribution is derived by assuming that the GRB rate as a function of redshift is proportional to the star formation rate. The SF2 model from Porciani & Madau (2001) is used in this analysis. We truncate the redshift distribution at 10. Based on these differential distributions, we obtain the cumulative distributions, p_x, where x is one of these parameters. We use the discrete forms of these distributions to save the calculation time. The bin sizes of $\log E_p$, $\log E_{\rm iso}$, and z are taken as 0.025, 0.1, and 0.01, respectively.

2. Simulate a GRB. We first generate a random number m ($0 < m \leq 1$) and obtain the value of x_m from the inverse function of $p_x(x_m) = m$, i.e., $x_m = p_x^{-1}(m)$. Since p_x is in a discrete form, we search for a bin i, which satisfies $p_x(x_i) < m$ and $p_x(x_{i+1}) > m$ and calculate the x_m value by $x_m = (x_{i+1} + x_i)/2$. Repeating this step for each parameter, we get a simulated GRB characterized by a set of parameters denoted as (z, $E_{\rm iso}$, E_p).

3. Calculate S_γ and examine whether or not the S_γ satisfies our threshold setting. The gamma-ray fluence is calculated by $S = E_{\rm iso}(1+z)/4\pi D_L^2(z)$, where $D_L(z)$ is the luminosity distance at z (for a flat universe with $\Omega_M = 0.3$). If $S < S_{{\rm th},\gamma}$, the burst is excluded.

4. Derive t_b. We first infer a t_b value from our empirical relation in a flat universe of $\Omega_M = 0.3$, then assign a deviation (Δt_b) to the t_b value. The distribution of Δt_b is taken as $dN/d\Delta\log t_b = \exp(-\Delta t_b^2/2\sigma)$, where $\sigma = 0.1$. This typical value is taken according to the current sample, which gives the mean and median deviations as $\sigma = 0.15$ and 0.11, respectively. If the t_b value is in the range of $0.4 < t_b < 6$ days, this burst is included in our sample. Otherwise, it is excluded.

5. Assign *observational errors* to E_p, S_γ, and t_b. Since the observed σ_x/x is about 10%–20%, we take the errors as $\sigma_x/x = 0.25k$ with a lower limit of $\sigma_x/x > 5\%$, where k is a random number between 0 and 1.

6. Repeat steps 2 and 5 to obtain a sample of 10^3 GRBs.

The distributions of z, E_p, and S_γ for the simulated GRB sample are shown in Figure 8 (*solid lines*). The observed distributions of these quantities are also shown for comparison (*dotted lines*). The observed redshift distribution is derived from the current GRB sample with known redshifts (45 GRBs). The observed E_p distribution is taken from Preece et al. (2000). The observed S_γ is derived from the BATSE current GRB sample[5] (Cui et al. 2005). The comparisons indicate that the mock GRB sample tends to be a softer (low E_p) and brighter (high S_γ) one. The redshifts of the mock GRB sample tend to be higher than the current GRB sample, but this might be due to observational biases against high-redshift GRBs (Bloom 2003).

[4] Our simulations do not sensitively depend on the $E_{\rm iso}$ distribution. We have used a random distribution between $10^{51.5}$ and $10^{54.5}$ ergs and found that the characteristics of our simulated GRBs sample are not significantly changed.

[5] See http://cossc.gsfc.nasa.gov/docs/cgro/batse/.

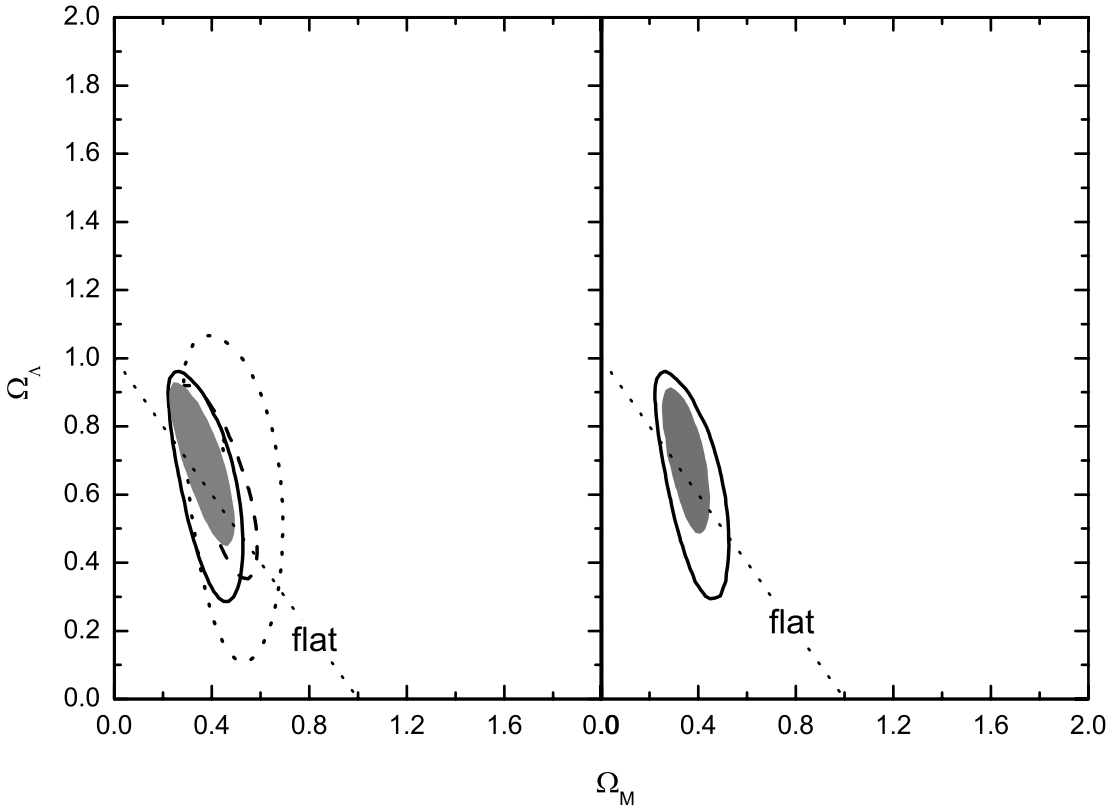

FIG. 9.—Comparison of the 1 σ likelihood contours for different simulated samples. *Left*: Simulations for different sample sizes, 25 GRBs (*dotted contour*), 50 GRBs (*solid contour*), 75 GRBs (*dashed contour*), and 100 GRBs (*shaded region*). The same observational errors ($\sigma_x/x = 0.25k$, where k is a random number between 0 and 1) are adopted. *Right*: Simulations for the same sample size (50 GRBs) but for different observational errors: $\sigma_x/x = 0.25k$ (*solid contour*) and $\sigma_x/x = 0.15k$ (*shaded region*; see the procedure of our simulations for details). The dotted line is for a flat universe.

We investigate the effect of the sample size on the cosmological constraints with our mock GRB sample. We randomly select subsamples of 25, 50, 75, and 100 GRBs from the mock GRB sample. We compare the 1 σ contours of likelihood distributions in the $(\Omega_M, \Omega_\Lambda)$-plane derived from these subsamples in the left panel of Figure 9. It is evident that as the sample size increases, the constraint on Ω_M and Ω_Λ becomes tighter. Comparing the left panel of Figure 9 with Figure 8 in Riess et al. (2004), we find that the likelihood contour derived from the subsample of 50 GRBs is comparable to that derived from the gold sample of 157 SNe Ia.

Precision cosmology requires accurate observations. Modern sophisticated observation techniques in distant SNe Ia (e.g., Riess et al. 1998; Schmidt et al. 1998; Perlmutter et al. 1999) and cosmic microwave background (CMB) fluctuations (e.g., Bennett et al. 2003; Spergel et al. 2003) have made great progress on modern precision cosmology. We inspect the uncertainties of the distance modulus derived from the SNe Ia data and find that the average uncertainty is $\bar{\sigma}_{\rm DM} \sim 0.25$, while for our GRB sample it is 0.45. Increasing observational precision (i.e., reducing the errors) should significantly improve the constraints on the cosmological parameters. We simulate another GRB sample with systematically smaller *observational errors*, i.e., $\sigma_x/x = 0.15k$ in step 5 of our simulation procedure. We get a sample with $\bar{\sigma}_{\rm DM} \sim 0.28$, comparable to the SNe Ia gold sample. The comparison of the likelihood contours (1 σ) in the $(\Omega_M, \Omega_\Lambda)$-plane derived from a sample of 50 mock GRBs with $\bar{\sigma}_{\rm DM} \sim 0.45$ (*solid contour*) and with $\bar{\sigma}_{\rm DM} \sim 0.28$ (*shaded region*) is shown in the right panel of Figure 9. It is found that the latter is significantly tighter, comparable to that derived from a sample of 100 mock GRBs with an average error in modulus of 0.45.

The results in Figure 9 indicate that tighter constraints on cosmological parameters could be achieved by either enlarging the sample size or increasing the observational precision. If a sample of 50 GRBs with comparable observational precision to that of the SN Ia gold sample could be established, the constraints would be even tighter than those derived from the SN Ia gold sample.

6. CONCLUSIONS AND DISCUSSION

Without imposing any theoretical models or assumptions, we investigate the relationship among $E_{\gamma,\rm iso}$, E'_p, and t'_b using a multivariable regression method. Our GRB sample includes 15 bursts, whose E'_p and t'_b are well measured. The results indicate that $E_{\gamma,\rm iso}$ strongly depends on both E'_p and t'_b with a very small dispersion, e.g., equation (5) for a flat universe with $\Omega_M = 0.28$. We also perform a similar analysis by replacing $E_{\gamma,\rm iso}$ by the isotropic afterglow energies in the X-ray and optical bands and find that these energies are essentially not related to E'_p and t'_b at all. We then use the $E_{\gamma,\rm iso}(E'_p,\ t'_b)$ relationship as a luminosity indicator to infer the possible cosmological implications from the GRB sample. Since this relationship is cosmology-dependent, we suggest a new method to weight various cosmology-dependent relationships with its probability of being the right one and use the cosmology-weighted standard candle to explore the most plausible cosmological parameters. Our results show that the most probable values are $(\Omega_M,\ \Omega_\Lambda) = (0.28,\ 0.64)$. At the 1 σ level, we have $0.05 < \Omega_M < 0.50$ and $\Omega_\Lambda < 1.2$. In the case of a flat universe, the 1 σ constraints are $0.13 < \Omega_M < 0.49$ and

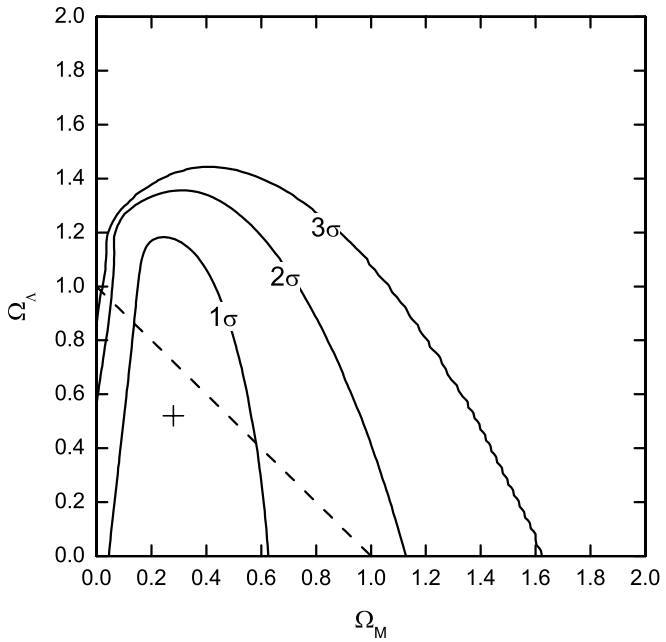

FIG. 10.—Contours of likelihood interval distributions in the $(\Omega_M, \Omega_\Lambda)$-plane derived by the marginalization method. The cross marks the most probable value of $(\Omega_M, \Omega_\Lambda)$, which is (0.28, 0.52). The contours give $0.05 < \Omega_M < 0.61$ (1 σ). Considering a flat universe (*dashed line*), the contours yield $0.14 < \Omega_M < 0.58$ and $0.40 < \Omega_\Lambda < 0.84$ (1 σ).

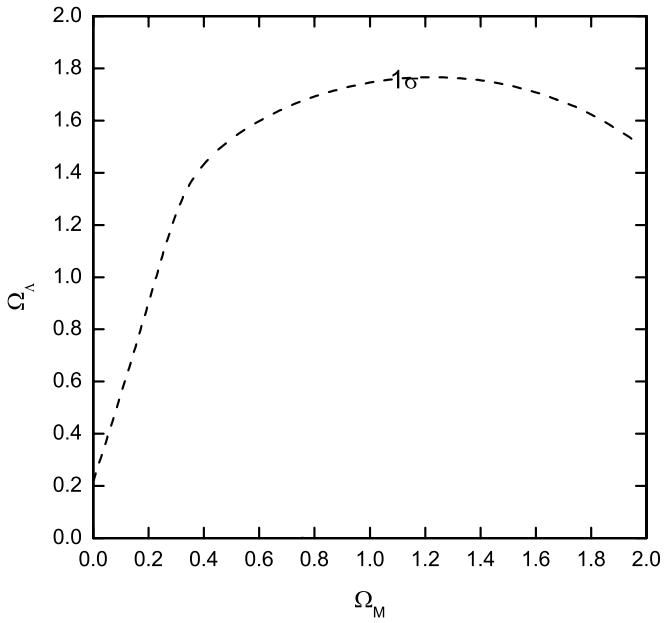

FIG. 11.—Same as Fig. 5, but the uncertainties of the parameters in the empirical relationships are also included in the error of the distance modulus in the calculation of $p(\Omega)$ by eq. (12). Only the 1 σ interval is shown.

$0.50 < \Omega_\Lambda < 0.85$. The deceleration factor of the universe (q) and its cosmological evolution (dq/dz) are also investigated with an evolutionary form of $q = q_0 + z\,dq/dz$. The GRB sample implies that the most probable values of (q_0, dq/dz) are (-1.00, 1.12), and they are constrained in the ranges of $-2.23 < q_0 < 0.26$ and $-0.07 < dq/dz < 3.48$ at the 1 σ level. A transition redshift between the deceleration and the acceleration phases of the universe is inferred as $\hat{z}_t = 0.78^{+0.32}_{-0.23}$ at the 1 σ level from the GRB sample.

As a luminosity indicator, our model-independent $E_{\gamma,\mathrm{iso}}(E_p', t_b')$ relationship has the advantage over the previous Ghirlanda relation that only pure observational data are involved. Since this luminosity indicator is cosmology-dependent, we use a strategy through weighting this relationship in all possible cosmologies to statistically study the cosmography and cosmological dynamics. A similar method has been used in the SN cosmology when dealing with the uncertainty in the present Hubble constant H_0. In their method (e.g., Riess et al. 1998), the systematic error of H_0 is not included when calculating the error of the distance modulus. Rather, they integrated the probability of H_0 over a large range of values (without weighting for each value of H_0). This is the so-called marginalization method. We also perform this marginalization method to deal with our coefficients (κ_0, κ_1, and κ_2) and redo the cosmology analysis. This is equivalent to integrating over the whole cosmology parameter space without weighting, i.e.,

$$p(\Omega) = \int_{\bar{\Omega}} p(\bar{\Omega}|\Omega)\, d\bar{\Omega}. \qquad (17)$$

The result using this method to constrain Ω_M and Ω_Λ is presented in Figure 10. Comparing it with Figure 5, we find that both methods give consistent results, but Figure 5 gives a tighter constraint on cosmological parameters. This is understandable, since the weighting method reduces the contributions of side lobe around the "true" cosmologies. In any case, an essential ingredient of both methods is that the uncertainty of the standard candle itself is not included in calculating the uncertainty of the distance modulus derived from the data. If the uncertainty of the standard candle is indeed included in the uncertainty of the distance modulus, with equations (12) and (17) to calculate $p(\Omega)$, one gets a very loose constraint (Fig. 11). Even at the 1 σ level, the current GRB sample cannot place any meaningful constraints on both Ω_M and Ω_Λ. We believe, however, that in such a treatment, the uncertainty of the distance modulus is overestimated, since the error introduced from measurements should not be mixed with the systematic uncertainty of the standard candle.

The GRB sample from which our relationship is drawn is currently small. The constraints on the cosmological parameters derived from this sample are weaker than those from the SN Ia gold sample. Our simulations indicate that either enlarging the sample size or increasing the observational precision could greatly improve the constraints on the cosmological parameters. A sample of 50 bursts with the current observational precision would be comparable to the 157 SN Ia gold sample in constraining cosmology, and a better constraint is achievable with better observational precisions or an even larger sample size.

Our simulations also indicate that the GRB sample satisfying our relationship observationally tends to be a soft and bright one, for which t_b' is in the reasonable range for detection. Detailed optical afterglow light curves covering from a few hours to about 10 days after the burst trigger[6] are required to measure the t_b value. The observed t_b ranges from 0.4 to 5 days in the current GRB sample. In the *CGRO*/BATSE duration table,[7] there are ~1500 long GRBs. To test the probability of a BATSE burst having a t_b in the range of 0.4–5 days, we perform a

[6] Starting from about 10 days, the contributions from the underlying SN and host galaxy components may become prominent, and the afterglow level may be too faint to be detected.

[7] See http://gammaray.msfc.nasa.gov/batse/grb/catalog/current.

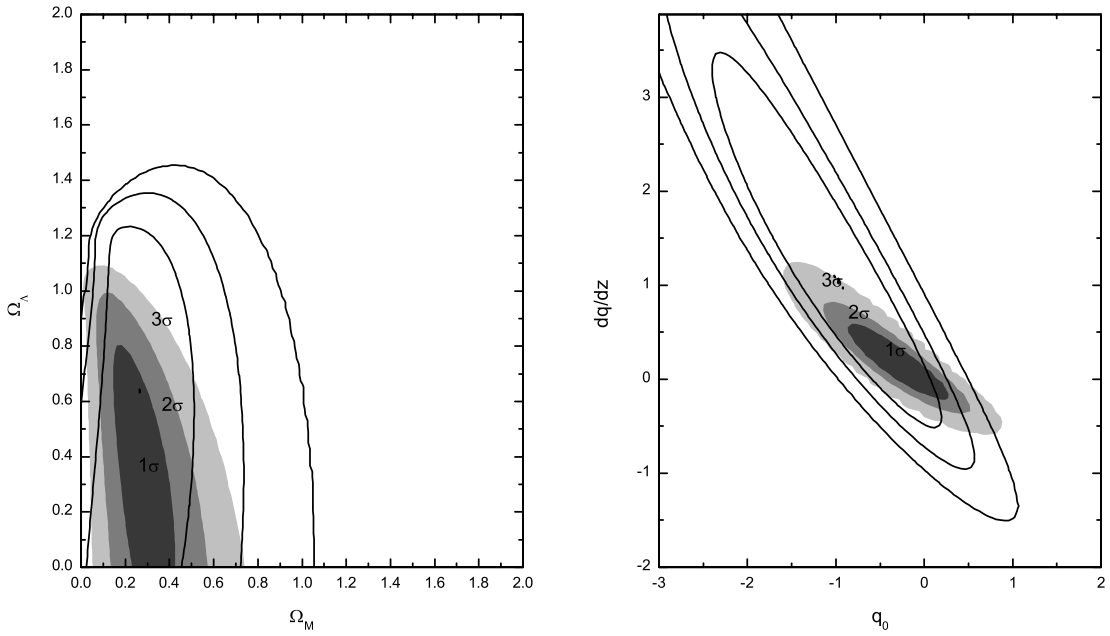

FIG. 12.—Demonstration of the potential constraints on cosmological parameters with high-redshift GRBs. The gray contours show the results derived from five pseudo–high-redshift GRBs together with the observed GRB sample (1 σ [*dark gray*] to 3 σ [*light gray*]), and the line contours show the results from the current observed GRB sample only.

simulation similar to that described in § 5, but take the E_p and S_γ distributions directly from the BATSE observations. We find that the probability is $\sim$0.15 in the cosmology of $\Omega_M = 0.3$ and $\Omega_\Lambda = 0.7$. Among well-localized GRBs, about 50% of the bursts are optically bright. We thus estimate that there have been $\sim$110 BATSE GRBs that might have been detected to satisfy our $E_{\gamma,\rm iso}(E'_p,\ t'_b)$ relationship. As shown in Figure 9, such a sample is comparable to the SNe Ia gold sample for constraining cosmological parameters. A dedicated GRB mission carrying a BATSE-like GRB detector and having the capability of precisely localizing and following up GRBs (like *Swift*) would be ideal to establish a homogenous GRB sample to perform precision GRB cosmology (Lamb et al. 2005b).

Since launched on 2004 November 20, the *Swift* mission (Gehrels et al. 2004) is regularly detecting GRBs with a rate of $\sim$80 bursts per year. Detailed X-ray and UV/optical afterglow observations spanning from 1 minute to several days after the burst have been performed for most of the bursts. However, the energy band of the *Swift* Burst Alert Telescope (BAT) is narrow, i.e., 15–150 keV. As we show in Figure 8, the typical E_p of a burst in our sample is marginally at the end of the BAT energy band. As a result, BAT is not ideal for the purpose of expanding the sample for GRB cosmology. As a result, we do not expect a dramatic enlargement of our sample in the *Swift* era. Nonetheless, those bursts with an E_p of $\sim$50–100 keV[8] could have their E_p well-measured by *Swift*. We therefore highly recommend detailed optical follow-up observations for these bursts with UVOT and/or other ground-based optical telescopes. This would present an opportunity to enlarge our sample with the *Swift* data.

The major advantage of GRBs serving as a standard candle over SNe Ia is their high-redshift nature. The observed spectra and fluences of high-redshift GRBs may not be too different from the nearby ones (Lamb & Reichart 2000). For example, the fluence of GRB 000131 ($z = 4.5$) is 1×10^{-5} ergs cm^{-2} in the 25–100 keV band (Hurley et al. 2000), which is significantly larger than the fluence of typical GRBs ($\sim10^{-6}$ ergs cm^{-2} in the 25–2000 keV band). The highest redshift burst in our sample is GRB 020124 ($z = 3.2$). Its fluence is 6.8×10^{-6} ergs cm^{-2} in the 30–400 keV band, and its observed peak energy is 120 keV. These indicate that the current GRB missions, such as *Swift* and *HETE-2*, are adequate to observe high-redshift GRBs.[9] We explore how the constraints on cosmological parameters are improved by identifying several high-redshift bursts. We artificially select five high-redshift GRBs from our simulated GRB sample with $z \sim 4.0$, 5.0, 6.0, 7.0, and 8.0, respectively, and with observational errors $\sigma_x/x = 0.25k$. The constraints on the cosmological parameters from these pseudo–high-z GRBs together with the current observed GRB sample are shown in Figure 12 (*shaded region*), where the results from the current observed GRB sample are also plotted for comparison (*contours*). It is found that adding a few high-z GRBs could result in much tighter constraints on cosmological parameters. Identifying high-z GRBs and measuring their E'_p and t'_b are therefore essential for the GRB cosmology in the near future.

Our model-independent relationship is close to the Ghirlanda relationship, which was derived on the basis of a simple version of GRB jet models. In such a model invoking a jet with energy uniformly distributed in the jet cone, the observable t_b is physically related to the epoch when the bulk Lorentz factor of the ejecta is reduced to the inverse of the jet opening angle (Rhoads 1999; Sari et al. 1999). Relating *tb* to the jet opening angle, the jet energy is then given by $E_{\rm jet} \propto (E_{\gamma,\rm iso}t'_b)^{3/4}(n\eta_\gamma)^{1/4}$, where n is the circumburst medium density and η_γ is the efficiency of GRBs. The Ghirlanda relation can be then expressed

[8] Such a burst tends to be an X-ray–rich GRB (Lamb et al. 2005a).

[9] Strictly speaking, we refer to the optical band in the cosmological rest frame to define t'_b. This is not an issue if the GRB redshift is small. For high-z GRBs, the optical band in the observer's frame is highly extincted by neutral hydrogen, but one could still detect t_b from the infrared band. Infrared-band observations are also essential for identify high-z GRBs. IR follow-up observations are therefore essential to add the high-z bursts in our sample.

as $E_{\rm iso} \propto E_p'^2 t_b'^{-1} (n\eta_\gamma)^{-1/3}$. Comparing this with our model-independent relationship (eq. [5]), we can see that both relations are roughly consistent with each other if n and η_γ are universal among bursts. As discussed above, the motivations for us to introduce our multivariable relationship are twofold. First, n and η_γ may not be constant and actually vary from burst to burst. This introduces a lot more uncertainties in the Ghirlanda relationship (e.g., Friedman & Bloom 2005). Second and more importantly, there is no straightforward interpretation of the relation within the jet model. Jumping out from the jet model framework would give more freedom of theoretical interpretations.

The tight relation of $E_{\rm iso}(E_p',\ t_b')$ is very intriguing, and its physical reason calls for investigation. The fact that $E_{\gamma,\,\rm iso}$ strongly depends on E_p' and t_b', while both $E_{\rm XA,\,iso}$ and $E_{\rm OA,iso}$ do not, implies that t_b' is a quantity related to GRBs rather than to their afterglows. A similar signature was previously found by Salmonson & Galama (2002), who discovered a tight correlation between the pulse spectral lag of GRB light curves and t_b. We therefore suspect that t_b might be a unique probe for the GRB prompt emission properties. Within the jet scenario, the anticorrelation between t_b and $E_{\gamma,\,\rm iso}$ (first revealed by Frail et al. 2001) may be physically related to the different metallicity abundances of the progenitor stars (e.g., metal-poor stars rotate more rapidly, and the GRBs they produce are more energetic and have more collimated jets; MacFadyen & Woosley 1999; Ramirez-Ruiz et al. 2002) or may be simply a manifestation of the viewing angle effect in a structured-jet scenario (Rossi et al. 2002; Zhang & Mészáros 2002b). Such an anticorrelation, when combined with the physical models of $E_{\gamma,\,\rm iso}-E_p$ correlations (e.g., Zhang & Mészáros 2002a; Rees & Mészáros 2005), may be able to interpret the observed $E_{\rm iso}(E_p',\ t_b')$ relation, although a detailed model is yet constructed. Alternatively, there might be a completely different physical reason under the $E_{\rm iso}(E_p',\ t_b')$ relation that is not attached to the jet picture. One possibility is that the spectral break in the prompt emission and the temporal break in the optical band may be related to a same evolving break in the electron spectral distribution (B. Zhang, 2005, in preparation). In such an interpretation, the temporal break time in the optical band is expected to be different from those in the radio or in the X-ray bands. Since so far there is no solid proof for the achromatic nature in broadband for any "jet break," such a possibility is not ruled out.

We are grateful to the anonymous referee for valuable comments. We also thank Z. G. Dai, D. Xu, Y. Z. Fan, X. F. Wu, G. Rhee, D. Lamb, G. Ghirlanda, D. Lazzati, T. Piran, Y. P. Qin, and B. B. Zhang for helpful discussions. This work is supported by NASA grant NNG04GD51G, a NASA *Swift* GI (Cycle 1) program, and the National Natural Science Foundation of China (grant 10463001).

REFERENCES

Amati, L. 2003, Chinese J. Astron. Astrophys., 3, 455
Amati, L., et al. 2002, A&A, 390, 81
Andersen, M. I., et al. 2003, GCN Circ. 1993, http://gcn.gsfc.nasa.gov/gcn/gcn3/1993.gcn3
Band, D. L., & Preece, R. D. 2005, ApJ, 627, 319
Barth, A. J., et al. 2003, ApJ, 584, L47
Bennett, C. L., et al. 2003, ApJS, 148, 97
Berger, E., et al. 2002, ApJ, 581, 981
———. 2003, Nature, 426, 154
Björnsson, G., et al. 2001, ApJ, 552, L121
Bloom, J. S. 2003, AJ, 125, 2856
Bloom, J. S., Frail, D. A., & Kulkarni, S. R. 2003a, ApJ, 594, 674
Bloom, J. S., Morrell, N., & Mohanty, S. 2003b, GCN Circ. 2212, http://gcn.gsfc.nasa.gov/gcn/gcn3/2212.gcn3
Bromm, V., & Loeb, A. 2002, ApJ, 575, 111
Butler, N. R., et al. 2003, GCN Circ. 2007, http://gcn.gsfc.nasa.gov/gcn/gcn3/2207.gcn3
Ciardi, B., & Loeb, A. 2000, ApJ, 540, 687
Cui, X., Liang, E., & Lu, R. 2005, AJ, 130, 418
Dai, Z. G., Liang, E. W., & Xu, D. 2004, ApJ, 612, L101
Dai, Z. G., & Lu, T. 2002, ApJ, 580, 1013
Djorgovski, S. G., et al. 1998, ApJ, 508, L17
———. 1999, GCN Circ. 510, http://gcn.gsfc.nasa.gov/gcn/gcn3/510.gcn3
———. 2003, Proc. SPIE, 4834, 238
Eichler, D., & Levinson, A. 2004, ApJ, 614, L13
Fenimore, E. E., & Ramirez-Ruiz, E. 2000, preprint (astro-ph/0004176)
Firmani, C., Ghisellini, G., Ghirlanda, G., & Avila-Reese, V. 2005, MNRAS, 360, L1
Frail, D. A., et al. 2001, ApJ, 562, L55
———. 2003, ApJ, 590, 992
Friedman, A. S., & Bloom, J. S. 2005, ApJ, 627, 1
Gehrels, N., et al. 2004, ApJ, 611, 1005
Ghirlanda, G., Ghisellini, G., & Lazzati, D. 2004a, ApJ, 616, 331
Ghirlanda, G., et al. 2004b, ApJ, 613, L13
Gou, L. J., Mészáros, P., Abel, T., & Zhang, B. 2004, ApJ, 604, 508
Greiner, J., Guenther, E., Klose, S., & Schwarz, R. 2003, GCN Circ. 1886, http://gcn.gsfc.nasa.gov/gcn/gcn3/1886.gcn3
Halpern, J. P., et al. 2000, ApJ, 543, 697
Hjorth, J., et al. 2003, ApJ, 597, 699
Holland, S. T., et al. 2002, AJ, 124, 639
———. 2003, AJ, 125, 2291
———. 2004, AJ, 128, 1955
Hurley, K., et al. 2000, GCN Circ. 529, http://gcn.gsfc.nasa.gov/gcn/gcn3/529.gcn3
Jakobsson, P., et al. 2003, A&A, 408, 941
———. 2004a, A&A, 427, 785
———. 2004b, ApJ, 617, L21
Jimenez, R., Band, D. L., & Piran, T. 2001, ApJ, 561, 171
Klose, S., et al. 2004, AJ, 128, 1942
Kulkarni, S. R., et al. 1999, Nature, 398, 389
Lamb, D. Q., Donaghy, T. Q., & Graziani, C. 2005a, ApJ, 620, 355
Lamb, D. Q., & Reichart, D. E. 2000, ApJ, 536, 1
Lamb, D. Q., et al. 2005b, astro-ph/0507362
Liang, E. W., Dai, Z. G., & Wu, X. F. 2004, ApJ, 606, L29
Lin, J. R., Zhang, S. N., & Li, T. P. 2004, ApJ, 605, 819
Lloyd, N. M., Petrosian, V., & Mallozzi, R. S. 2000, ApJ, 534, 227
Lloyd-Ronning, N. M., & Zhang, B. 2004, ApJ, 613, 477
MacFadyen, A. I., & Woosley, S. E. 1999, ApJ, 524, 262
Marshall, F. E., Markwardt, C., & Swank, J. H. 2003, GCN Circ. 2052, http://gcn.gsfc.nasa.gov/gcn/gcn3/2052.gcn3
Marshall, F. E., & Swank, J. H. 2003, GCN Circ. 1996, http://gcn.gsfc.nasa.gov/gcn/gcn3/1996.gcn3
Martini, P., Garnavich, P., & Stanek, K. Z. 2003, GCN Circ. 1980, http://gcn.gsfc.nasa.gov/gcn/gcn3/1980.gcn3
Metzger, M. R., et al. 1997, Nature, 387, 879
Möller, P., et al. 2002, A&A, 396, L21
Mortsell, E., & Sollerman, J. 2005, J. Cosmol. Astropart. Phys., 506, 4
Nakar, E., & Piran, T. 2005, MNRAS, 360, L73
Norris, J. P., Marani, G. F., & Bonnell, J. T. 2000, ApJ, 534, 248
Paczynski, B. 1998, ApJ, 494, L45
Panaitescu, A., & Kumar, P. 2002, ApJ, 571, 779
Pedersen, K., Fynbo, J., Hjorth, J., & Watson, D. 2003, GCN Circ. 1924, http://gcn.gsfc.nasa.gov/gcn/gcn3/1924.gcn3
Perlmutter, S., et al. 1999, ApJ, 517, 565
Porciani, C., & Madau, P. 2001, ApJ, 548, 522
Preece, R. D., Briggs, M. S., Mallozzi, R. S., Pendleton, G. N., Paciesas, W. S., & Band, D. L. 2000, ApJS, 126, 19
Price, P. A., et al. 2003, ApJ, 589, 838
Qin, Y. P., et al. 2005, preprint (astro-ph/0502373)
Ramirez-Ruiz, E., Lazzati, D., & Blain, A. W., 2002, ApJ, 565, L9
Rees, M. J., & Mészáros, P. 2005, ApJ, 628, 847
Reichart, D. E., et al. 2001, ApJ, 552, 57
Rhoads, J. E. 1999, ApJ, 525, 737
Riess, A. G., et al. 1998, AJ, 116, 1009
———. 2004, ApJ, 607, 665
Rossi, E., Lazzati, D., & Rees, M. J. 2002, MNRAS, 332, 945
Sakamoto, T., et al. 2004, ApJ, 602, 875

Sakamoto, T., et al. 2005, ApJ, 629, 311
Salmonson, J. D., & Galama, T. J. 2002, ApJ, 569, 682
Sari, R., Piran, T., & Halpern, J. P. 1999, ApJ, 519, L17
Schaefer, B. E. 2003, ApJ, 588, 387
Schmidt, B. P., et al. 1998, ApJ, 507, 46
Spergel, D. N., et al. 2003, ApJS, 148, 175
Stanek, K. Z., et al. 1999, ApJ, 522, L39
Tiengo, A., Mereghetti, S., & Schartel, N. 2003a, GCN Circ. 2241, http://gcn.gsfc.nasa.gov/gcn/gcn3/2241.gcn3
———. 2003b, GCN Circ. 2285, http://gcn.gsfc.nasa.gov/gcn/gcn3/2285.gcn3
Totani, T. 1997, ApJ, 486, L71
Vreeswijk, P., Fruchter, A., Hjorth, J., & Kouveliotou, C. 2003, GCN Circ. 1785, http://gcn.gsfc.nasa.gov/gcn/gcn3/1785.gcn3
Vreeswijk, P. M., et al. 2001, ApJ, 546, 672
Weidinger, M., U. J. P., Hjorth, J., Gorosabel, J., Klose, S., & Tanvir, N. 2003, GCN Circ. 2215, http://gcn.gsfc.nasa.gov/gcn/gcn3/2215.gcn3
Wu, X. F., Dai, Z. G., & Liang, E. W. 2004, ApJ, 615, 359
Xu, D. 2005, preprint (astro-ph/0504052)
Xu, D., Dai, Z. G., & Liang. E. W. 2005, ApJ, 633, 603
Yamazaki, R., Ioka, K., & Nakamura, T. 2004, ApJ, 606, L33
Zhang, B., & Mészáros, P. 2002a, ApJ, 581, 1236
———. 2002b, ApJ, 571, 876